16

Large Area a-Si/μc-Si Thin Film Solar Cells

Fan Yang
Qualcomm MEMS Technologies, Inc.
United States

1. Introduction

Providing a sustainable and environment friendly energy source, photovoltaic (PV) power is becoming ever-increasingly important, as it decreases the nation's reliance on fossil-fuel generated electricity. Though widely regarded as a clean and renewable energy source, large scale deployment of PV is still impeded by the fact that the cost of PV energy is generally higher compared to grid electricity. Current development of PV technology is focused on two aspects: 1) improving the efficiency of PV modules and systems and 2) lowering the cost of delivered electricity through decreasing the manufacturing and installation cost. The merit of commercial solar cells aiming at terrestrial application is justified by the cost of unit PV power generation, dollar per watt ($/Wp), where Wp stands for the peak power generated by the cells.

Since the first practical PV cell grown on Si wafer at the Bell Laboratory in 1954, PV technology has been developed for more than five decades and evolved three "generations" based on different PV materials. The first generation of solar cells use crystalline materials, where the cost of the bulk materials has hit the point that further cost reduction is very difficult (Green 2007). In contrast, the second generation cells use thin film materials, where the required amount of materials is merely a few percent of that of bulk materials, significantly reducing the fabrication cost of this type of cells. The emerging, third generation of PV technology applies new materials and novel device concepts aiming at even higher efficiency and lower cost. At this moment, the commercial PV market is dominated by the first and second generation PV modules, and the third generation cells are still under lab research. As shown in Fig. 1, the efficiency of thin film PV system has improved from ~4 % in 1995 to >11 % in 2010, and will keep increasing to ~12% by 2020, a three-fold improvement compared to the system efficiency back in 1995. During the same timeframe, the cost of thin film PV system drops from ~4 $/Wp to ~0.5 $/Wp. Crystalline PV systems, though with higher efficiencies, have higher cost, i.e. 2.5 times the cost of thin film PV system. From the cost and material supply point of view, thin film solar cells will have a long-term development and gradually take more market share from the crystalline cells.

Many thin film materials can be used for PV cells, e.g., Si, CdTe, CIGS or the emerging organic/polymeric materials. Comparing to other materials, thin film Si, including amorphous Si (a-Si) and microcrystalline Si (μc-Si), have the following characters:

1. The PV active Si is the most abundant solid state element on the earth's shell, allowing for practically unlimited production of Si cells.

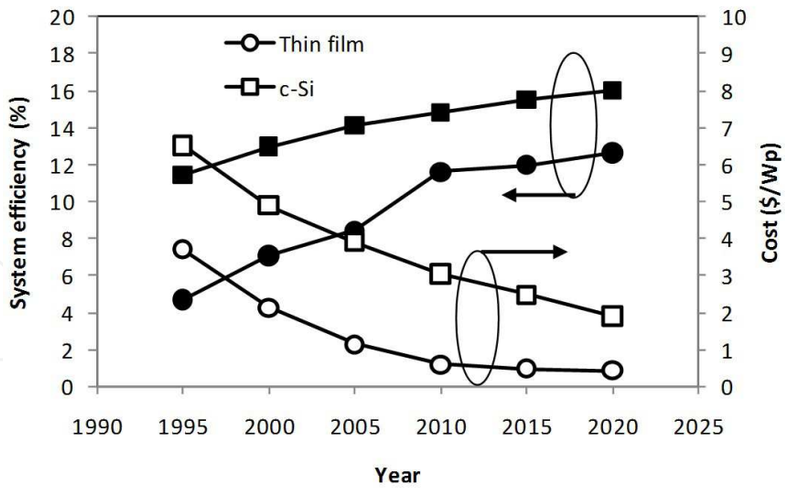

Fig. 1. Photovoltaic (PV) system efficiency and cost. Data from the U.S. Department of Energy.

2. Si has no toxicity and is environmental friendly.
3. Process of a-Si/μc-Si thin films takes the advantage of the highly mature semiconductor and display industries.
4. a-Si is a metastable material, and the initial cell performance of a-Si based cells degrades under illumination and then stabilizes, known as the Staebler–Wronski effect (Kolodziej 2004).

In addition, production of a-Si/μc-Si solar panels has a low entry barrier, thus making it more acceptable for the emerging PV manufactures. The first thin film Si solar cells were put into production in the 1980's when they were used as power sources for small electronic gadgets. Volume production of a-Si based solar panels started after the year 2000 with the introduction of large-area chemical vapor deposition (CVD) process at these companies: Sharp Corporation, United Solar Ovonic, Kaneka, Mitsubishi Heavy Industries, Ltd, etc. The true burst of Si thin film solar cells, on the other hand, came after 2007 with the "turnkey" (ready to use) thin-film solar manufacturing equipments introduced by Unaxis SPTec (later Oerlikon Solar) (Meier et al. 2007) and Applied Films Gmbh & Co. (later part of Applied Materials Inc.) (Repmann et al. 2007). The idea is that instead of developing the film deposition and module manufacturing technologies by self, the would-be solar maker can buy the full set of equipments together with the process recipes, and start manufacturing panels with relative ease. Each having a designed capacity of 40 – 60 MW, over twenty "turnkey" systems were sold to solar module makers world wide by Oerlikon and Applied Materials by 2010. The fast expansion of production capacity directly induced the drop of a-Si/μc-Si panel cost from around 5 $/Wp to less than 2 $/Wp.

At the moment thin film Si cells, including a-Si and μc-Si, take the largest market share (more than half of total production volume) among all types of thin film cells. Close to 5 GW of a-Si/μc-Si panels were manufactured in 2010, and will keep similarly large market share to at least 2013 (Fig. 2) (Young 2010). It is also noted from the same figure that the production volume of a-Si panels has an impressive compound annual growth rate (CAGR) of 42%, highest among all thin film PV technologies. Currently a significant amount of Si thin film panels are single-junction a-Si panels, whose efficiency will gradually increase to 8% - 8.5%. By adopting the a-Si/μc-Si multi-junction cells, panel efficiency will move up to

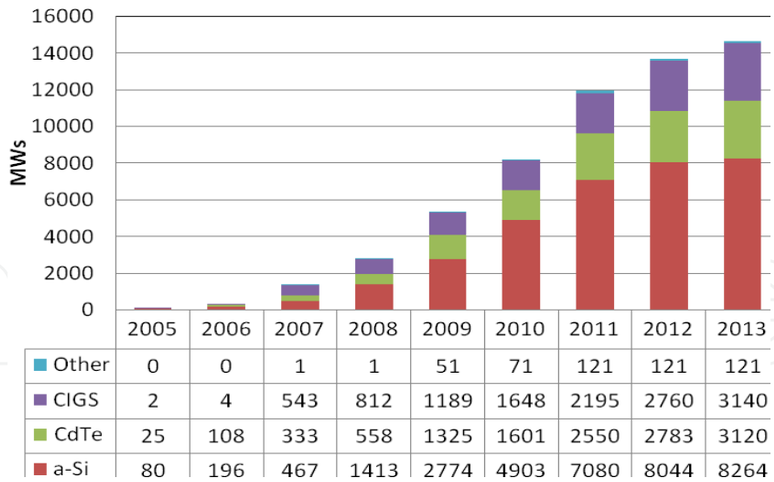

	2005	2006	2007	2008	2009	2010	2011	2012	2013
Other	0	0	1	1	51	71	121	121	121
CIGS	2	4	543	812	1189	1648	2195	2760	3140
CdTe	25	108	333	558	1325	1601	2550	2783	3120
a-Si	80	196	467	1413	2774	4903	7080	8044	8264

Fig. 2. Global thin film solar panel manufacturing capacity and compound annual growth rate (CAGR) by technology, 2006-2013 (estimate) (Young 2010).

around 10% after 2012. Costs for these technologies are expected to range from 0.80 to 1.20 $/Wp (Mehta 2010). Consequently, the energy cost pay-back time of these panels will be shortened to 0.5-2 years.

For the above mentioned reasons, a-Si/µc-Si solar panels are the mostly produced among all thin film technologies and will stay in large volume production the foreseeable future. This chapter introduces the fundamental thin film PV solar cell structure, the energy conversion physics, and state-of-the-art large scale solar panel manufacturing. Various methods of performance enhancement and cost reduction of large area thin film Si solar cells are focuses of this chapter.

This chapter is organized as follows. Section 1 briefly introduces the history and current production status of a-Si and µc-Si solar panels. Section 2 analyzes the cost structure of typical thin film solar panels and systems. The basic solar cell structures, including the PV active Si p-i-n junction layers and the front and back contact layers, are discussed in Section 3. Next, we describe in details the panel production process in Section 4 and 5. The front end of line (FEOL) processis first introduced, with discussions on CVD deposition of Si layers, physical vapor deposition (PVD) process of transparent conductive oxide (TCO) layers and back contacts, and laser scribing steps. The back end of line (BEOL) process is then described with the introduction of module fabrication, bus line wiring and panel encapsulation. Different process flow configurations are also compared in this part. We summary the chapter in Section 5.

2. Cost structure of PV system

To begin the discussion of the cost of solar panels, we split the cost of thin film PV system into four major parts:

1. Planning and financing: 15%
2. Inverter: 9-10%
3. Balance of system (BOS) and installation: 10-30%
4. Module: 40-66%

Sharing similar cost percentage of the first three parts with crystalline Si PV systems, the much lower module cost gives thin film PV system lower overall cost and a higher development potential. An increase or decrease of the efficiency of the module implies an increment or a reduction of the BOS and installation costs, respectively. Nevertheless, the financing and inverter cost remain always the same. Therefore, the use of lower efficiency thin film modules are financially more favorable in those cases in which the value of the installed area is not relevant. Thin film panels are thus more applicable to the PV electricity power plants built in remote areas like deserts. Large volume production and deployment is the key factor to fully demonstrate the financial benefit of thin film solar modules.
The cost of thin film modules, in turn is composed of five major components (Jäger-Waldau 2007):

1. Material cost (40%). The material consumption is determined by the film growth technology (e.g., PVD vs. CVD), and is also dominated by the module packaging and assembly technology. Special, TCO-coated glass substrates take a significant portion of the direct material cost (25-40%). Assuming similar technology used, the materials cost is inversely proportional to the production volume and panel efficiency.
2. Equipment related (capital) spending (20%). Initial investment on equipment on a-Si/μc-Si thin film panel manufactures is generally expensive. Upon fixed initial equipment investment, the annual depreciation of equipments is dominated by the deposition materials. The equipment depreciation rate is inversely proportional to the process throughput and module efficiency.
3. Labor cost (15-17%). The layered, monolithically integrated panel structure minimizes human operation, and the highly automated production methods used in the state-of-the art thin film PV panel manufactures reduce the labor cost. For a given total production volume, the labor cost is inversely proportional to the process throughput, extent of automation, and production module efficiency.
4. Energy consumption (15%). Modern PV manufactures use a significant amount of energy to run the factory, including machinery power consumption used for manipulating the substrate, controlling of substrate temperatures, RF power generators, film deposition system, vacuum system, exhaust handling, laser tool, lighting, air conditioning, etc. Once a factory is set up, a large amount of the overhead energy consumption is fixed, and the energy consumption per module is inversely proportional to the process throughput.
5. Freight (7-9%). The logistics of shipping and handling of the raw material as well as the assembled module panels take a larger portion of cost in thin film solar panels compared to their crystalline counter parts due to their greater size and weight. Unlike the other factors, freight cost is relatively constant for each panel.

As seen from the relationship of the thin film PV module cost structure summarized in Fig. 3, the process technology determines the direct material and energy consumption, equipment depreciation and ultimately the panel efficiency, which in turn affect the panel cost. In another word, more advanced module process technology leads to both higher panel efficiency and lower panel cost. Thus in this chapter, we put our focus on the process details of the manufacturing of modern, large-area a-Si/μc-Si solar panels.

3. Basic thin film Si solar cell structure

Typical a-Si single junction solar cells are composed of five principal layers: Si p-i-n diode sandwiched between two conductive layers. The front TCO forms the front contact, and the

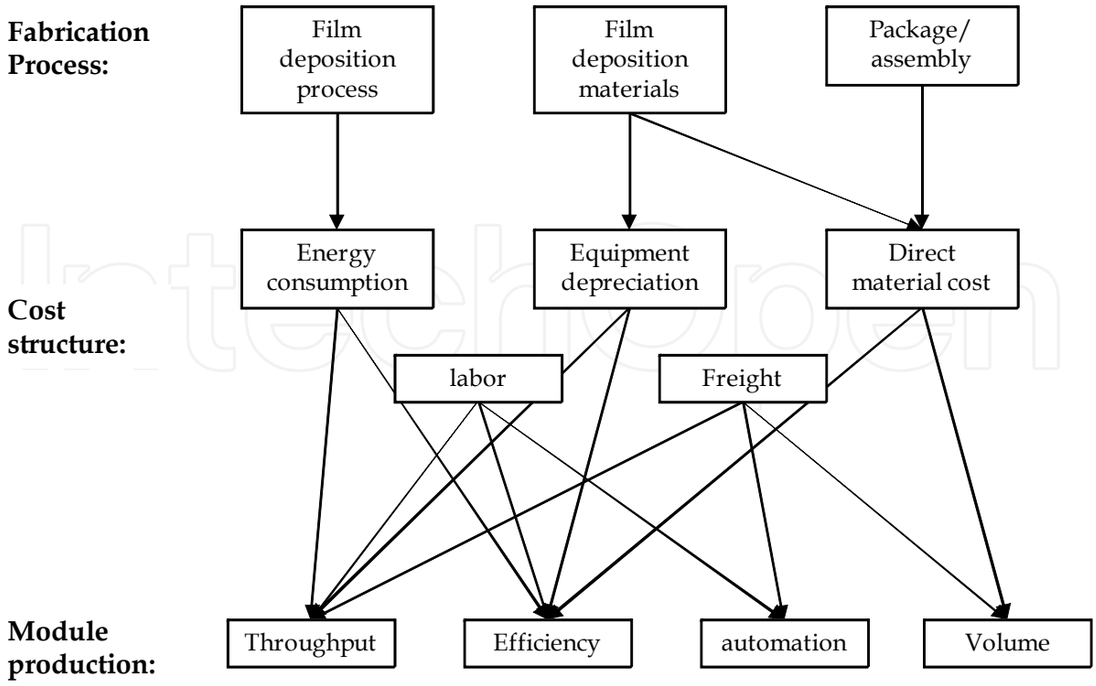

Fig. 3. Relationship between fabrication process, cost structure, and production of thin film PV modules.

back TCO and the reflector form the back contact (Fig. 4). The Si p-i-n junction absorbs sun light and generates photocarriers, which are collected by the conductive, front and back contacts. The substrate (e.g., glass) provides mechanical support for all the layers. Stacking two a-Si/μc-Si cells on top of each other forms the tandem junction structure, which is also sandwiched between the front and back TCOs.

Depends on the type of substrates on which the films are grown, there are basically two kinds of cell structures. 1) "Substrate" structure, where none-transparent substrates, i.e., metal foils, are used for growing the film stack. Sun light enters the cell from the top of the film stack by going through the top TCO. 2) "Superstrate" structure, where transparent substrates like glass or plastic films are used. Sun light enters the cell through the transparent glass/plastics and the TCO layer. The growth order of the Si p-i-n diodes are reversed in the two structures. The monolithically integrated superstrate type solar cells have superb encapsulation and compatibility with conventional electrical and safety regulations, thus holding a dominant market share.

3.1 PV active Si p-i-n layers

The Si p-i-n junction is where the sun light is absorbed and converted to charge carriers, i.e., electrons and holes. Differs from crystalline Si (c-Si), a-Si for PV and other applications (e.g., thin film transistor, TFT) are actually hydrogenated amorphous silicon alloy (a-Si:H, here noted as a-Si for simplicity), in which the H atoms passivate the otherwise high-density Si dangling bonds in pure amorphous Si film that introduce trap states and severely affect the film electrical properties. Normally the H content can be as high as a few percent. The a-Si completely loses the periodical atomic lattice structure; instead, the Si atoms randomly

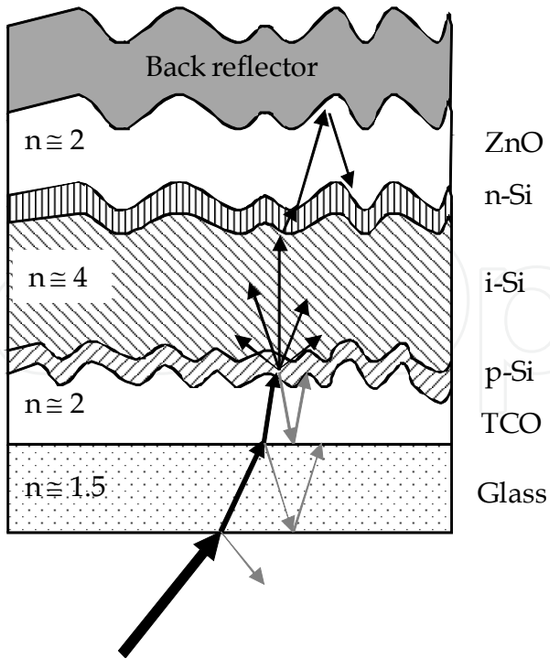

Fig. 4. Schematic single junction p-i-n a-Si solar cell. *n* stands for the index of refraction.

arrange in space. The lack of lattice structure makes a-Si a direct band gap semiconductor with a band gap of 1.8-1.9 eV at room temperature.

Hydrogenated microcrystalline Si (μc-Si:H, noted as μc-Si for simplicity) has a more complex, phase-mixed structure that consists of the crystalline phase made of silicon nanocrystallites and the amorphous Si matrix. The nanocrystallites grow into conglomerate clusters perpendicular to the film surface, whose diameters are typically between 10 and 50 nm. Embedded in amorphous silicon, the conglomerates are separated by a-Si, grain boundaries and micro-cracks. The band gap of μc-Si is 1.11 eV at room temperature, roughly the same as crystalline Si.

Photon absorption is proportional to the wavelength-dependent absorption coefficient, α, of the film. For typical a-Si and μc-Si, α is between 10^2 and 10^5 cm^{-1} in the visible range (Shah et al. 2004), which is 10-50 times larger than that of c-Si. Large α naturally allows for thinner absorber in solar cells. In the a-Si/μc-Si i-layer, an absorbed photon excites an electron from the valance band to the conduction band, creating a free electron and leaving a hole in the valance band. Due to the amorphous nature of a-Si and μc-Si films, the electrons and holes haves limited diffusion length and short life time. Electronic carrier transport properties are normally characterized by the mobility × lifetime product (μτ-product), which is the physical characteristic of both carrier drift and diffusion processes. The measured products of the electron mobility and lifetime, $\mu^0\tau^0$, is 2×10^{-8} cm^2/Vs for a-Si and 1×10^{-7} cm^2/Vs for μc-Si, respectively, much lower than those measured in c-Si wafers (Beck et al. 1996; Droz et al. 2000). The low μτ-product in a-Si or μc-Si makes the p-n diode configuration that is widely used in c-Si solar cells unsuitable with these materials, as the photocarrier collection in a p-n diode is diffusion limited. To avoid electron and hole recombination, p-i-n junction is used, where the built-in field drifts electrons towards the n-layer and holes towards the p-layer. The measured electron diffusion length is 2 μm in a-Si and 10 μm in μc-Si under the filed of

10^4 V/cm, comparable to or larger than the thickness of the solar cell film stack. As a result, the p-i-n type cells have efficient carrier collection efficiency.

Photons absorbed in the heavily doped n- and p- layers, however, don't contribute to the photocurrent as there is no net electric field in the doped layers. As a result, the n- and p-layers are usually less than 20 nm thick to limit photon absorption in these "window" layers. Further reduction of photon absorption in realized by increasing the band gaps of the n- and p-layers, e.g., doping the a-Si or μc-Si window layers with carbon so that they are transparent to the portion of the solar spectrum to be harvested in the i-layer. Total thickness of a typical single or tandem junction cell is less than 2 μm, which is only a few percent thick of a c-Si cell.

3.2 Front and back contacts

Though not PV active, the front and back contact layers play important roles on the cell performance. Optical wise, the transparent TCO layers scatter the incident sun light and enhance the optical absorption inside the i-layer. Electrical wise, since the lateral conductance of thin, doped p/n silicon layers is insufficient to prevent resistive losses, the TCO contact layers conduct the photocurrent in the lateral direction to the panel bus lines. The TCO layers used for thin film solar cells are doped wide band gap semiconducting oxides.

For efficient material usage and fast film deposition, the a-Si/μc-Si absorbers are so thin that the incoming light will not be completely absorbed during one single pass for normal incident rays. Hence, for all absorber materials, optical absorption inside the silicon layers has to be enhanced by increasing the optical absorption path. The difference of index of refraction between the TCO layers and the Si layers, plus the rough interface induce diffusive refraction of incoming light at oblique angles, thus increasing the optical path of solar radiation (Fig. 4). This is typically done by nano-texturing the front TCO electrode to a typical root-mean-square (rms) surface roughness of 40–150 nm and/or nano-textured back reflectors. In the ideal case, these rough layers can introduce nearly completely diffusive transmission or reflection of light (Müller et al. 2004).

When applied at the front contact, TCO has to possess a high transparency in the spectral region where the solar cell is operating (transmittance > 90% in 350 – 1000 nm), strong scattering of the incoming light, and a high electrical conductivity (sheet resistance < 20 Ω/sq.) (Fortunato et al. 2007). For the superstrate configuration where the Si layers are deposited onto a transparent substrate (e.g., glass) covered by TCO, it has to have at the same time favorable physicochemical properties for the growth of the silicon. For example, the TCO has to be inert to hydrogen-rich plasmas, and act as a good nucleation layer for the growth of the a-Si/μc-Si films. For all thin-film silicon solar cells, scattering at interfaces between neighboring layers with different refractive indices and subsequent trapping of the incident light within the silicon absorber layers is crucial to high efficiency.

TCO is also used between silicon and the metallic contact as a part of the back reflector to improve its optical properties and act as a dopant diffusion barrier. The back TCO layer also prevents reaction between the metal and the a-Si/μc-Si underlayers. Furthermore, applied in a-Si:H/μc-Si:H tandem solar cells, TCO can be used as an intermediate reflector between top and bottom cells to increase the current in the thin amorphous silicon top cell (Yamamoto et al. 2006). Finally, nano-rough TCO front contacts act as an efficient antireflection coating due to the refractive index grading at the TCO/Si interface.

The front and back TCO layers are at the same time electrodes that collect photogenerated carriers. As a semiconductor, the optical transparency and the electrical conductivity are closely related to the band gap structure of the TCO. The short-wavelength cutoff of the transmission spectrum corresponds to the oxide band gap, whereas the long-wavelength transmission edge corresponds to the free carrier plasma resonance frequency. On the other hand, electron conduction in TCO is achieved by degenerate doping that increases the free carrier density and moves the Fermi level into the conduction band. High carrier density and carrier mobility are thus required for TCO layers. There is, however, a tradeoff between high optical transmittance and low electrical resistance. Increasing electron carrier density decreases resistivity but also increases the plasma oscillation frequency of free carriers, thus shifting the IR absorption edge towards the visible. The transmission window is thus narrowed as a result of improved conductivity.

TCO type	ITO	ZnO:Al	SnO_2:F
Optical transmission (350-1000 nm)	95%	90-95%	90%
Resistivity (Ω·cm)	$1\text{-}5\times10^{-4}$	$3\text{-}8\times10^{-4}$	$6\text{-}10\times10^{-4}$
Work function (eV)	4.7	4.5	4.8
Band gap (eV)	~3.7	~3.4	4.1-4.3
Deposition methods	RF sputtering	RF sputtering, LPCVD	APCVD, spray pyrolysis
Surface roughness	Flat	Excellent	Excellent
Plasma stability	Low	Excellent	Good
Relative cost	High	Middle	Low

Table 1. Different TCOs employed in Si thin film solar cells. RF, radio frequency. LPCVD, low-pressure chemical vapor deposition. APCVD, atmosphere-pressure CVD.

The most-widely used TCOs in Si thin film solar cells are doped SnO_2 (i.e., SnO_2:F) and ZnO (i.e., ZnO:Al) due to their temperature and chemical stabilities. Compared to the more conductive alternative indium-tin-oxide (ITO), they offer a much lower cost by avoiding the use of the costly In. At the same time, surface roughness induced by the crystalline texture of SnO_2 and ZnO is widely applied for increasing the optical absorption. These three typical TCOs are compared in Table 1.

The reflector layer on top of the back TCO can be Ag, Al, or white paint in a "superstrate" cell, and is the metal foil itself or another Ag/Al coating on the foil in a 'substrate' type cell. Ag is typically used in laboratory research work, while Al is more often used in mass production modules due to its lower cost and better properties in removing module shunts. Back contacts of Oerlikon's thin film panels, on the other hand, use proprietary white paint as the reflector (Meier et al. 2005). The white paint can be rolled on or screen printed directly onto the TCO. At the same time, it offers the following advantages (Berger et al. 2007): 1) high optical reflectance over a broad wavelength band, 2) optimal light scattering pattern which is generally beneficial for solar cells because this maximizes the fraction of photons that are trapped inside the solar cell due to total internal reflection at both cell surfaces, 3) pigmented materials have the potential of low cost. In certain instances, the white paint is a better surface reflector than Al, or TCO/Al reflector.

4. Factory panel production

As previously discussed (c.f., Section 2), manufacturing of the solar panels directly determines the cost of modules, which takes 40-66% of the overall PV system cost. This section focuses on the factory panel production, and addresses various methods of panel efficiency improvement and cost reduction.

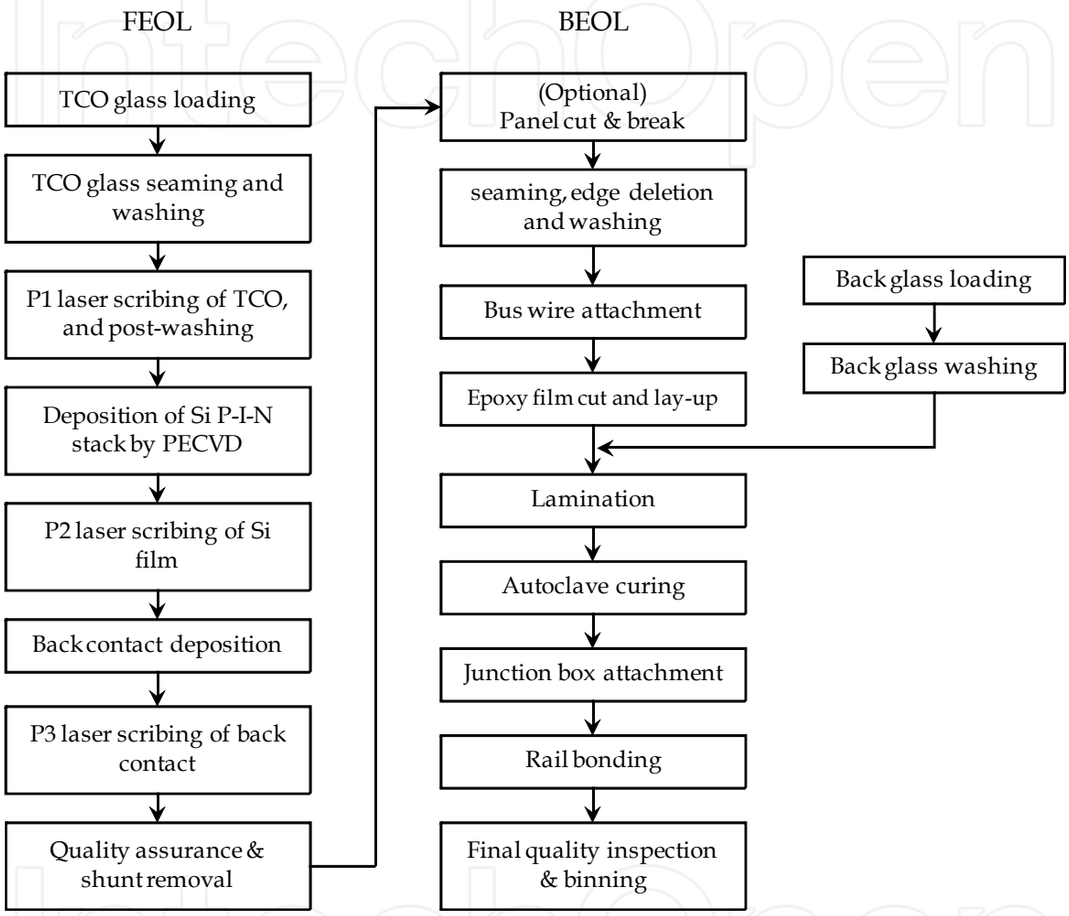

Fig. 5. Flow diagram of typical thin film solar panel production, comprising of both the front end of line (FEOL) and back end of line (BEOL) technologies and processes (Bhan et al. 2010).

Development in the a-Si and μc-Si thin film process technology combined with the booming PV market resulted in the fast expansion of a-Si/μc-Si based solar panel manufacturing after 2007. This industry largely benefits from the lab demonstration of thin film solar cells on small size substrates, as well as the large-area thin film deposition techniques developed for thin-film transistor liquid crystal display (TFT-LCD) industry. The growth of high-quality Si thin films for PV applications shares many of the skill sets required for growing Si TFT films, and using similar large-area thin film deposition chambers (Yang et al. 2007). In fact, both thin film solar "turnkey" equipment providers, Oerlikon and Applied Materials, have been manufacturing large-scale TFT-LCD deposition systems for years before becoming thin film solar equipment providers.

The general process flow of thin film panel fabrication is shown in the diagram of Fig. 5. This is a typical Applied Materials Sunfab process configuration (Bhan et al. 2010), though that of Oerlikon (Sun et al. 2009) and other 'superstrate' type panel makers are similar. The entire process is divided into the FEOL steps where the front glass substrate is deposited with active layers, and BEOL steps where the module is encapsulated. The FEOL mainly involves several film deposition and patterning steps, including the growth of Si p-i-n junctions by CVD and the growth of TCOs and metal layers by PVD. Laser scribing steps are used in between film depositions to form monolithically interconnected cells across the entire substrate. In the BEOL steps, the front glass with blanket film deposited during FEOL is cut, shaped and encapsulated to make solar panels. Optical and electrical inspections are taken upon finishing of FEOL for quality control purposes. Process of the 'substrate' type module shares many of the FEOL and BEOL steps, and the differences are discussed later in Section 4.3.

4.1 Front end of line (FEOL) process

The first step of module deposition involves loading of substrates in FEOL. Either float glass or TCO-coated glass is used, though an extra TCO growth step is required for the former case (Kroll et al. 2007; Sun et al. 2009). To prevent the glass from chipping and cracking during the following thermal cycle steps, as the film deposition steps require substrate temperatures ranging from 150 to 250 °C, the glass edge is seamed and reinforced. Then the glass goes through washing and drying steps to thoroughly remove debris, particles and organic contaminants. Laser-scribing step P1 follows to form isolated TCO contact strips. After a second washing step, the TCO glass is loaded into the film deposition chambers for the growth of PV active layers.

4.1.1 Growth of a-Si/μc-Si layers

The PV active Si p-i-n film stack is normally grown by CVD from gaseous precursors. Several CVD deposition techniques have been developed for the deposition of a-Si/μc-Si layers, including plasma-enhanced CVD (PECVD) (Schropp and Zeman 1998), remote plasma enhanced CVD (RPECVD) (Kessels et al. 2001), and hotwire CVD (Schroeder 2003). Though efficient lab-size solar cells are made with various CVD techniques, PECVD is prevailingly used for current industrial, high-throughput thin film PV module fabrication, as it possesses advantages like high deposition rate, in-situ chamber cleaning, good control over film quality, and requires lowest substrate temperature.

A typical PECVD chamber is structured like the schematics in Fig. 6. The substrate is supported by a susceptor, directly facing a gas diffuser. Process gases (SiH_4, H_2 and dopant gases) are fed into the chamber and dispersed by the diffuser. The diffuser and the susceptor are charged at opposite radio frequency (RF) voltages, thus exciting plasma within the chamber. Commonly used RF plasma is excited at 13.56 MHZ or 40 MHz, while higher RF frequencies are also used (Nishimiya et al. 2008). Higher RF frequencies are reported to deposit Si film faster due to higher plasmornic excitation energy. On the other hand, higher frequency means shorter RF wavelength, potentially forming standing wave inside the chamber that can cause non-uniform plasma distribution and reduce the a-Si/μc-Si film uniformity.

Using silane (SiH_4) as the precursor gas, the deposition of a-Si/μc-Si films can be described as a four-step process (Schropp and Zeman 1998):

1. Primary gas phase SiH_4 decomposition. The plasma excites and decomposes the SiH_4 molecules into neutral radicals and molecules, positively and negatively charged ions, and electrons.

2. Secondary gas phase reaction. The reaction between molecules, ions and radicals (product of the previous step) generates reactive species and eventually large Si-H clusters, which are also called dust or power particles. The neutral species diffuse to the substrate, while the positive ions bombard the growing film and the negative ions are constrained within the plasma.
3. Film deposition. The radicals diffusing to the substrate interact with the substrate surface in various ways, like radical diffusion, chemical bonding, hydrogen sticking to the surface or desorption from the surface.
4. Formation of a-Si film. The actively growing film then releases hydrogen and relaxes into the Si network.

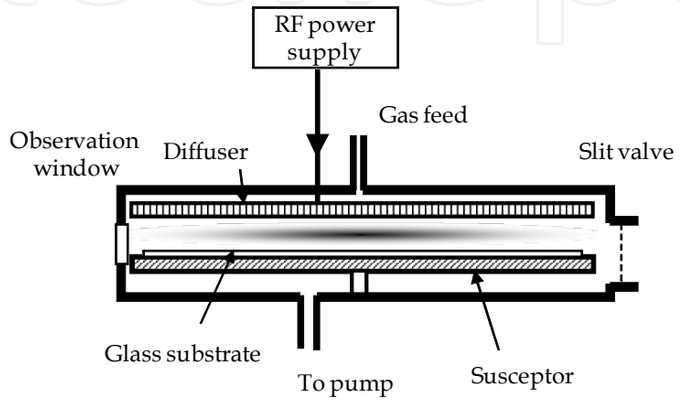

Fig. 6. Schematics of a PECVD process chamber.

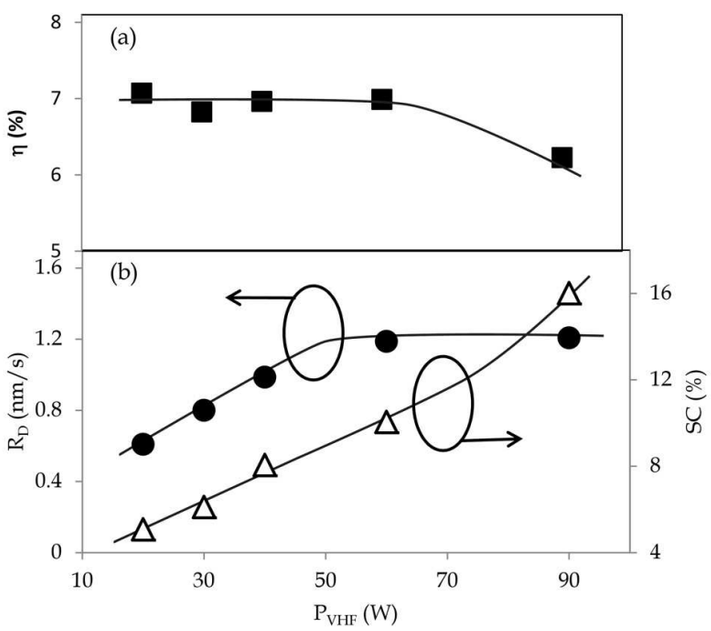

Fig. 7. Challenges met with high deposition rate (R_D) for PECVD grown µc-Si films. (a) Efficiencies of the optimal µc-Si single junction solar cell at different very-high frequency radio-frequency power (P_{VHF}). (b) Corresponding deposition rates RD and SiH_4 dilution concentration (SC) (Mai et al. 2005).

The overall film deposition is a complex process of gas and surface reactions, and is controlled by many deposition parameters, including gas composition, flow rate, chamber pressure, RF power density, RF frequency, substrate temperature, and the chamber size and geometry. Extensive studies are carried out to study the influence of those controlling parameters on the a-Si/μc-Si film properties, and are summarized in review papers (Luft and Tsuo 1993; Bruno et al. 1995). Perusing high solar energy conversion efficiency requires high quality, PECVD grown a-Si/μc-Si films, like high optical absorption, low dangling bond density, wide band gap for optical transmission of the p- and n- window layers (Schropp 2006).

Transferring the lab-developed process to solar panel production, however, has its own challenges. The PECVD steps take a significant portion of the cost in energy consumption and equipment depreciation (c.f., Fig. 3), thus substantial changes must be made to the lab-developed PECVD processes in panel manufacturing to fit the goal of lowering the panel cost. While maintaining the optimal panel performance, the widely adapted strategies are high rate of deposition (R_D) and large substrate size for high-throughput panel growth.

As previously discussed in Section 2, fast film deposition can lower the energy consumption, facilitating the throughput and process efficiency, thus effectively lower the cost of solar modules. The major obstacle to throughput increase is the μc-Si deposition, which has to be thick (> 1.5 μm) as limited by the finite absorption coefficient, thus requiring appreciably long deposition time. In fact, deposition of the μc-Si bottom cell in a-Si/μc-Si tandem junction solar panels takes the longest process time in the Oerlikon and Applied Materials process lines. To shorten the μc-Si deposition time and improve the overall throughput, research has been focused on increasing the deposition rate of μc-Si films.

Generally, increasing the density of SiH radicals promotes the growth of a-Si/μc-Si, thus increasing SiH_4 flow rate, applying higher RF power density, or using a higher RF excitation frequency all lead to higher R_D. For the simpler case of a-Si, higher RF power and higher gas flow rate result in faster film growth. As for the case of μc-Si, changing these deposition parameters at the same time affects the film crystallization in addition to increasing R_D. Since a good performed μc-Si solar cell needs to keep at the transition from microcrystalline to amorphous growth, increasing the film deposition rate should not be compromised by the film crystallinity. It is observed that increase of RF power requires higher SiH_4 concentration to keep the same crystallinity, which at the same time leads to higher deposition rate. In one example, Fig. 7 compared the high R_D achieved with increasing very high frequency (VHF) 94.7 MHz RF power (Mai et al. 2005). To maintain the maximum PV efficiency (Fig. 7a) at different VHF power (P_{VHF}), the silence concentration (SC) in the mixed gas has to increase with P_{VHF} (Fig. 7b). At small P_{VHF}, R_D increases linearly with P_{VHF}, and saturates around 1.2 nm/s when P_{VHF} is > 60 W. The solar cell efficiency, η stays constant for the same region since the μc-Si crystallinity remains unchanged. Further increase of P_{VHF} doesn't lead to higher RD, and the optimal cell efficiency drops at this region. It is important to note that higher deposition rate greatly improves the throughput of the panel manufacturing, and lowers the panel cost.

Since the merit of solar cell, $/Wp, is inversely proportional to the total solar module production (Hegedus and Luque 2003), growing solar cells over large-area substrates is one of the most efficient ways of lowering solar cell cost. For constant direct materials and labor cost, growing films over larger area substrates effectively lowers the module cost per unit area. The major challenge when scaling up the substrate is to maintain uniform film growth over large

area. Since various PECVD parameters directly affect the growth rate of a-Si / µc-Si film, the non-uniform distribution of these growth parameters induces local film thickness variation. For typical p-i-n type a-Si or µc-Si cells, the open circuit voltage (V_{OC}) and fill factor (*FF)* decrease upon increasing i-layer thickness, while J_{SC} increases as a result of the higher absorption in the thicker cells (Klein et al. 2002). Other than thickness, the RF power distribution affects the crystallinity of the as-grown µc-Si, which in turn changes the solar cell performance. For example, slight deviation of RF intensity resulted in unbalanced µc-Si crystallization in a Gen 8.5 PECVD chamber, as shown by the smaller fraction of crystallinity (FC) on the left side of chamber before adjusting the RF power supply feed (Fig. 8a), though such deviation could be too small to affect the a-Si and µc-Si film thicknesses (Yang et al. 2009). Small size a-Si/µc-Si tandem junction solar cells cut from the solar panels at corresponding locations, had non-uniform performance distribution. Sample cells from the low RF intensity side (left) had smaller short circuit current density (J_{SC}) (Fig. 8b) and higher V_{OC} (Fig. 8c) than those from the other side, while *FF* had a uniform distribution despite the RF influence (Fig. 8d). After modifying the RF feed of the PECVD chamber, balanced FC distribution was obtained, and the sample cells showed uniform distribution of J_{SC}, V_{OC} and *FF*. It is thus important to keep the uniform distribution of all process parameters in large scale process, and special attention must be paid to the RF power distribution across the whole chamber.

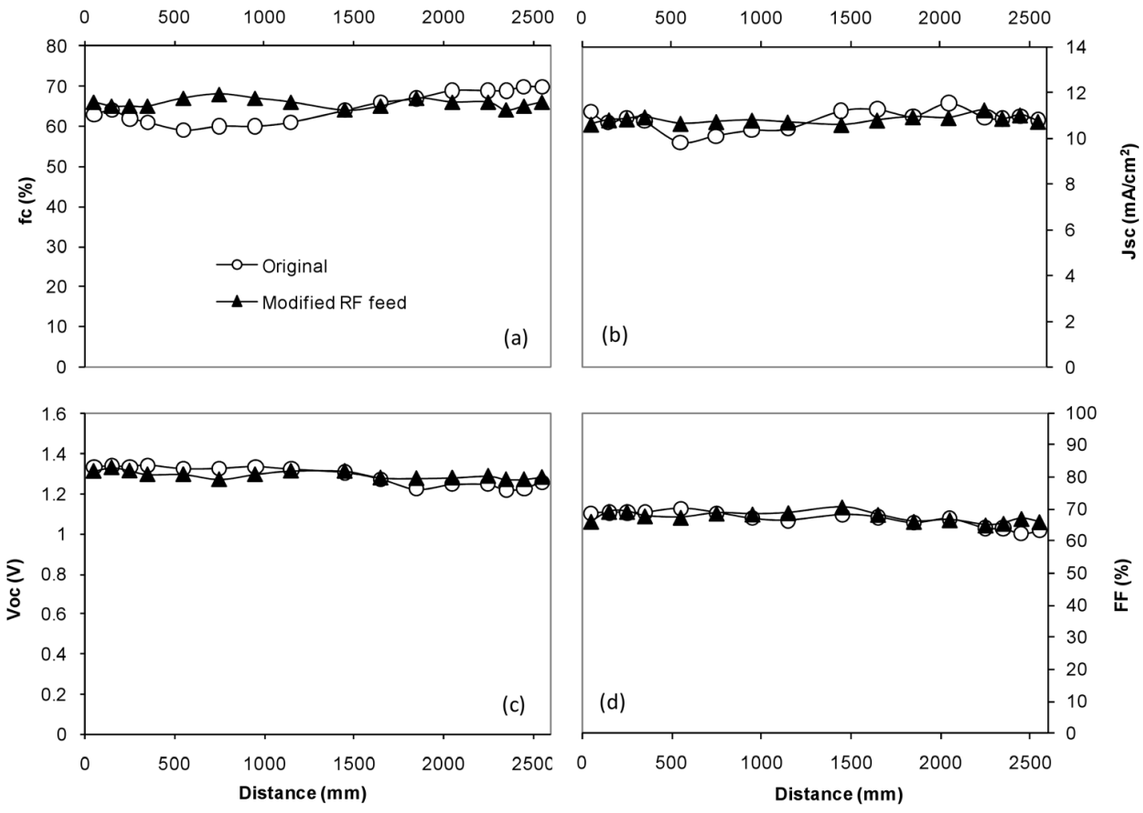

Fig. 8. µc-Si film uniformity and its impact to solar cell performance (a) Crystalline fraction (fc) change along substrate diagonal with original and modified RF feed. (b) J_{SC}, (c) V_{OC}, and (d) FF profiles along substrate diagonals. The two substrates were grown before and after modifying the RF feed location.

4.1.2 Growth of TCO layers

The TCO layers are typically grown by either CVD or PVD on industrial size substrates. Used as the front TCO layer, SnO_2:F layer are normally grown by CVD using $SnCl_4$ precursor gas on glass substrates (Rath et al. 2010). The finished SnO_2:F-coated glass is provided as substrates for later PECVD deposition of a-Si/μc-Si layers. Another front TCO candidate is AZO, which is usually grown by CVD processes using precursors like $Zn(C_2H_5)_2$ or sputter deposition (Agashe et al. 2004). Substrate temperatures are near 150 °C for the CVD deposition, and can go as high as 300 °C for sputtering.

For many solar panel manufactures, control of the front TCO properties, especially the surface roughness, can be financially unfeasible, thus purchasing glass substrate pre-coated with TCO becomes a good choice. For a-Si absorber layers a high transparency for visible light (wavelength λ = 400–750 nm) is sufficient, while for solar cells incorporating μc-Si the TCO has to be highly transparent up to the near infrared (NIR) region (400–1100 nm) to accommodate for the wider absorption spectrum of μc-Si. This imposes certain restrictions on the carrier density, *n*, of the TCO material, as increased free carrier absorption leads to a reduction of IR transmission (Agashe et al. 2004). SnO_2:F films fulfilling these requirements to a large extent, have been developed by Asahi Glass (Asahi Type U) (Sato et al. 1992). The ZnO crystallite facets imposes diffusive light scattering to the incident sun light, thus enhances the optical absorption with minimal absorbing layer. Further light trapping for long-wavelength light is also achieved in the Asahi high haze, HU-TCO glass, where the TCO surface has two types of textures of different characteristic length thus scattering different portions of light (Kambe et al. 2009).

The back TCO is typically AZO (c.f., Table 1), which is grown in-line with other in-house process steps. In addition, AZO provides excellent long-term stability as the back contact material. Since the back contact is grown on top of finished Si p-i-n stack, the substrate temperature should be kept low (<300 °C) to prevent the dopant diffusion from the a-Si/μc-Si n layers. The back AZO contact is typically grown by RF sputtering (Beyer et al. 2007) or low pressure (LP)-CVD (Meier et al. 2010) at temperatures < 150 °C.

4.1.3 Laser scribing

A big advantage of the superstrate type a-Si/μc-Si thin film solar panels lies in the monolithically integrated structure, which greatly reduces operational cost and increases production throughput and panel yield by eliminating connection of wafers in the fabrication of crystalline Si PV panels. The thin film panel is scribed into numerous small cells, which are interconnected in series for a high voltage output, which at the same time improves panel yield and lowers the resistive energy loss. The monolithically integrated series connection is realized by a three step patterning process that selectively removes the individual layers, i.e., TCO front contact, thin-film silicon layer stack, and back contact of the solar cell. Highly automated laser scribing patterning is widely used for all patterning steps (c.f., Fig. 5) as it provides precise positioning, high throughput and minimum area losses.

Scribing thin film layers into sections with laser has developed a mature technology applied to large-area superstrate-type module fabrication, where laser beam incidents through the glass substrate. As depicted in Fig. 9, laser scribing mechanism can be described as a four-step process (Shinohara et al. 2006).

1. Absorption of laser beam. By choosing appropriate laser energy/wavelength, the layer to be scribed absorbs the laser energy following Lambert's law, with more heat created

at the glass-side of the film (Fig. 9a). Typical laser energy is >1×10^6 W/cm^2, and calculation shows more than 80% of that energy is absorbed and converted to heat building up in the film.

2. Decomposition of H from a-Si:H. The absorbed heat induces the decomposition of a-Si:H, and releases hydrogen at a temperature of > 600 °C (Fig. 9b). In fact, the local temperature in the film can be heated up to 700 °C by the laser.
3. Destruction of the PV layers and back contact. The gaseous H_2 quickly expends its volume and pressure under the high temperature. The pressure of the H_2 gas can amount to >1×10^7 Pa, inducing enormous shear stress on the layers above the heated zone. In one estimation, applying a 532 nm, 12 kHz and 9.5 × 10^6 W/cm^2 laser beam on a-Si single junction module created shear stress of 3.9×10^8 Pa, enough to break the layers on top of the heating zone, among which the most ductile Ag layer has a shear strength of 10^7 – 10^8 Pa (Fig. 9c).
4. Formation of heat affected zone (HAZ). Along with the H_2 volume expansion, the film cracks quickly followed by blasting off, effectively removing the a-Si/µc-Si layers and the back contact layers above the local, heated zone. The laser heating also damages the film around the removed region, creating a HAZ with high density of defects and poor electrical properties (Fig. 9d). By using high-frequency pulsed laser, the HAZ is limited to less than a few tens of nm wide.

It is important to note that the laser scribing removal is not a true thermal process but the mechanical blasting off of the film. By applying different wavelengths of lasers, the laser energy is absorbed by different layers, thus selectively removes those layers without affecting other, underlying layers.

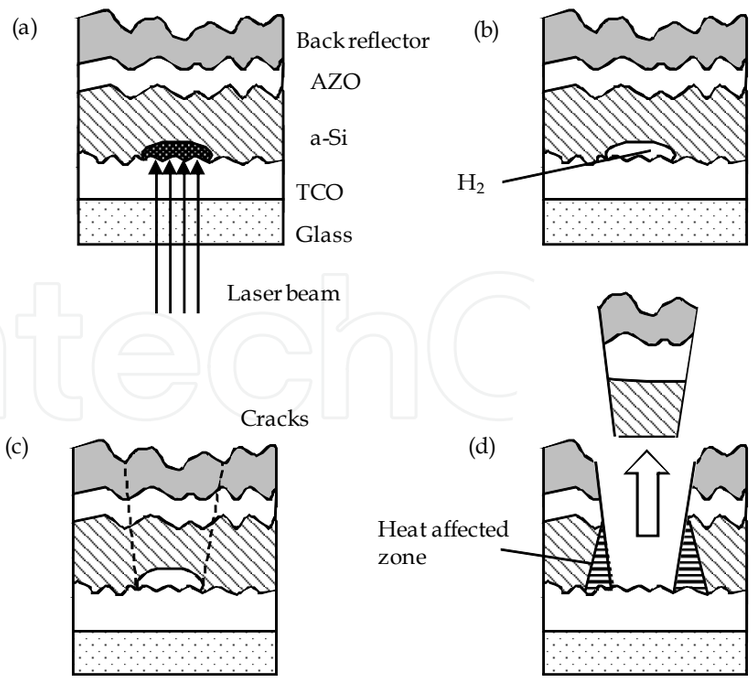

Fig. 9. Laser-scribing mechanism. (a) absorption of laser beam incidents through the glass, (b) decomposition of H from a-Si:H, (c) destruction of the photovoltaic layer and back electrode, (d) film blasted off and formation of heat affected zone (Shinohara et al. 2006).

Combination of several laser-scribed layers is used to create interconnection in Si thin-film modules (Fig. 10a). The cell strips are defined by selective ablation of individual layer stacks, and the interconnection between neighboring strip cells are provided by the overlap of conductive layers. In the microscope view of a typical interconnection area (Fig. 10b), P1 is the first laser scribing step that cuts through the front TCO layer, P2 is the second scribing step that cuts through the p-i-n junction layers, P3 is the last step that cuts through the junction layers and the back reflector. The dead-area, i.e., the narrow area between P1 and P3 lines including the HAZ, makes up the interconnection junction but doesn't contribute to photocurrent generation. State-of-the-art laser process can limit the interconnection width to < 350 μm to minimize the dead-area. For a-Si/μc-Si module production, the scribing laser is typically powerful Nd:YVO_4 solid-state laser with primary emission at 1064 nm and second harmonic generation at 532 nm. P1 is scribed by the 1064 nm irradiation, in which the strong absorption in TCO results in intensive local heating and explosive TCO evaporation (ablation); the glass that doesn't absorb in this wavelength keeps cool and is free from damage. P2 and P3 are similarly scribed by the 532 nm irradiation. As shown in Fig. 10c, the P3 laser cuts abrupt edges on the a-Si film without leaving any observable damage to the underlying TCO layer. The three laser scribing steps combining the subsequent film deposition steps form differences in the depths of different layers and conductive channels, forming the interconnection region of the cell strips' series connection. Power optimized, high-speed laser scribing technique is already applied in making 5.7 m^2 solar panels with exceptional performance (Borrajo et al. 2009).

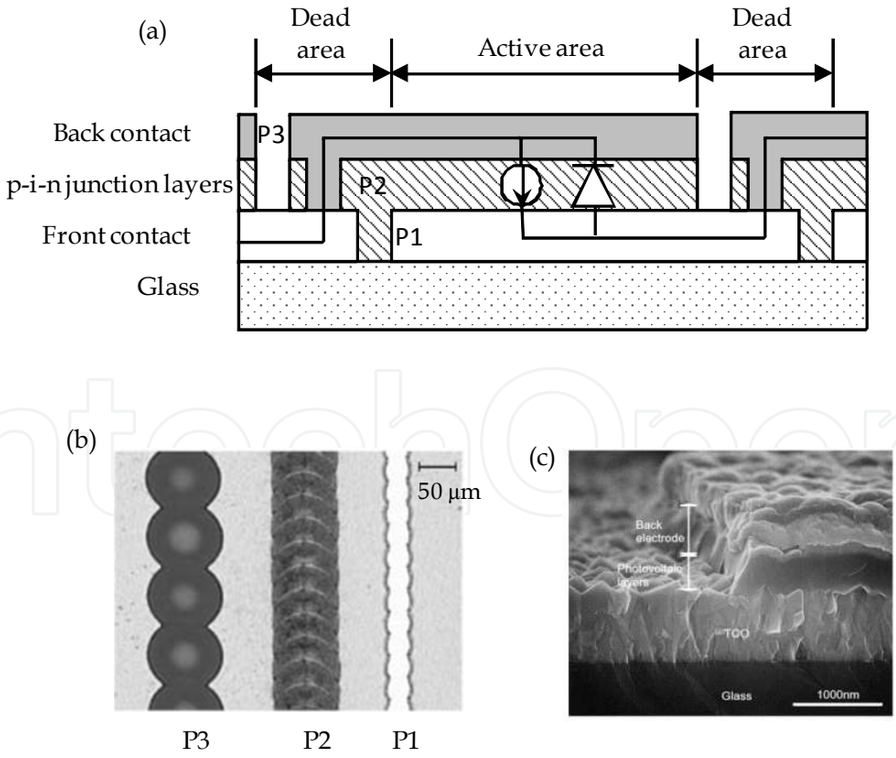

Fig. 10. (a) Schematic cross-sectional view of Si thin film solar panel showing the sectioned film and laser scribing lines (P1, P2 and P3). (b) Optical microscope image of the laser scribed lines. (c) Scanning electron microscope image of P3 scribed PV layer (Shinohara et al. 2006).

Making up the interconnection of cell strips, the laser scribing pattern is decisive to the assembled panel performance. Since the total panel area is fixed, the width of cell strips determined by the laser scribing pattern is inversely proportional to the number of cell strips. Laser scribing pattern also affects the number of junctions and total dead area, which both contribute to losses in panel power output. Thus design of the laser scribing pattern is optimized with the width of strip cells and the sheet resistance of the front and back contacts.
Precisely scribing fine lines that defines the monolithically integrated thin film solar module, laser scribing technology greatly enhanced the overall panel performance and improves the automation of the process flow. It is an important step in improving the module efficiency and driving down the module cost independent of the film deposition processes.

4.1.4 Rest of FEOL steps

After all film deposition and laser scribing steps conclude, the central PV active region is isolated from the panel edge to avoid electrical shock. In one way, the outside edge of the entire film stack is removed by 10-20 mm of width, called edge deletion. This is typically done by mechanical grinding or laser scribing (same as P2 laser).
To burn out the defects and improve panel yield, the final FEOL step involves removing cell shunts by reverse biasing the cells, or shunt busting. Shunting in Si thin film solar cells refers to high leakage current in reverse bias, which leads to a loss of power and efficiency. In large scale deposition, pinholes or locally thinner Si layer could form, which allow a connection between the top and bottom contacts, forming partially shorted PV diodes. When applying a reverse bias, larger current is focused at these shunt regions, resulting in local heat generation and consequent burning out of the low resistance pathway. Microscopic observation confirms the change of film morphology and its connection to the curing of the solar cells (Johnson et al. 2003).
As all cells are readily formed at this stage, electrical and optical inspection of individual cell strips are taken after the shunt busting for quality assurance purposes. This completes the FEOL processing of the solar panel.

4.2 Back end of line (BEOL) process

Panels fabricated at FEOL have to be further shaped and encapsulated to complete the solar panel module at the BEOL steps. Though no more film is deposited in the BEOL steps, these are important processes to ensure high quality solar panel production.

4.2.1 Module fabrication and bus line wiring

If the module size is smaller than the substrate, glass with deposited film is first scored and broken into the final panel size, and goes through edge deletion. Then the panel is thoroughly washed for another time and ready for final bus line soldering.
According to the laser scribing layout, the two terminal segments of the series connected cell strips are each soldered to a bus line. These two terminal segments serve as the beginning and ending of the series connection of all cell strips on the panel. The cross bus bars are then attached to the terminal bus line and leaves out the final electrical connection to the external circuit.

4.2.2 Module encapsulation

To stand for extreme weather conditions in field usage, the functional films, i.e., TCO layers, a-Si/µc-Si films, metal coatings, and bus lines need good encapsulation to achieve

for long panel lifetime. The most common encapsulation method for panels with the glass substrate is to use another piece of glass to cover the functional films. The gap between the two glass plates is filled with an epoxy (ethylene vinyl acetate, EVA, or polyvinyl butyral, PVB) film, which not only insulates the functional films against reactants like oxygen and moisture, but also mechanically strengthens the rigidness of the finished panel. Quality of the module encapsulation is directly associated with the failures of panels in the field. Judgment of the encapsulation properties includes low-interface conductivity, adequate adhesion of encapsulants to glass as a function of in-service exposure conditions, and low moisture permeation at all operation temperatures (Jorgensen et al. 2006).

The panel then passes through a laminator where a combination of heated nip rollers removes the air and seals the edges. The lamination film at the same time provides electrical insulation against any electric shock hazard. At the exit of the laminator conveyer, the modules are collected and stacked together on a rack for batch processing through the autoclave where they are subjected to an anneal/pressure cycle to remove the residual air and completely cure the epoxy. Finally, a junction box is attached to the cross bus wire and sealed on top of the hole of the back glass and is filled with the pottant to achieve a complete module integrity.

The fully processed module is then tested for output power, I_{SC}, V_{OC}, and other characteristics under a solar simulator. Then it is labeled, glued to the supporting bars, and packaged. At this point, the full panel assembly is finished.

4.3 Production process flow

Multiple chambers are used for deposition of different functional layers in the module production process. Optimizing the arrangement of chambers and controlling of the process flow are crucial to the production throughput and directly affect the panel production cost. There are mainly three types of process flows: batch process, continuous process and hybrid process. Characteristics of the three processes are compared in Table 2.

Batch process of film deposition is the most intuitive way of arranging deposition chambers. In this configuration, functional layers are deposited consequently onto batches of substrates. The typical batch processes are seen in Oerlikon's thin film production lines. An example is the Oerlikon KAI-20 1200 production system (Fig. 11a), which consists of two PECVD process towers, two load-locks, one transfer chamber and an external robot for glass loading from cassettes (Kroll et al. 2007). Each process tower is equipped with a stack of ten plasma-box-reactors where ten substrates are deposited simultaneously. The layers are processed in parallel at the same time in both stacks (2×10 reactors). The whole KAI-20 1200 PECVD production system shares one common gas delivery system including the mass flow controllers and one common process pump system. Engineering work has been put to ensure small box-to-box variations of deposition rates, layer thickness uniformities. The batch process normally requires small footprint, and is suitable for slow deposition that requires long process time (e.g., the absorbing i-layers). In fact the PECVD deposition of different p-, i-, and n- layers can be combined within the same chamber as long as dopant diffusion from the process chamber can be minimized. In most cases more than one chambers are used for the entire film stack, thus when they are moved between separate chambers the substrate manipulation and heating / cooling time has to be minimized to increase the process throughput.

Process flow types	Batch Process	Continuous Process	Hybrid Process
Schematics	Fig. 12a	Fig. 12b	Fig. 12c
Examples	Oerlikon Solar customers	United Solar, ECD, Xunlight	Applied Materials customers
Production volume	20 MW/yr	30 MW/yr	40-55 MW/yr
System footprint	6 m × 8.6 m (KAI 1200)	6 m × 90 m	Variable sizes
Substrate	Glass, 1.1 m × 1.25 m	Stainless steel roll, 36 cm x 2.6 km	Glass, 2.2 m × 2.6 m
Operational flexibility	Same equipment can be used for multiple depositions	Moderate operational flexibility but often leads to inefficient capital use.	Same equipment can be used for multiple depositions
Standardized equipment	Easily modified to produce different solar cell structures	Recipe of the entire line is fixed. Equipments are optimized for minimal operating conditions	Easily modified to produce different solar cell structures.
Rate of deposition affects throughput	Favors slow depositions that require long residence time.	Slow depositions require large equipments and slow process flow.	Slow process is shared by parallel chambers for high throughput.
Processing efficiency	Requires strict scheduling and control. Minimal energy integration.	Reduces fugitive energy losses by avoiding multiple heating and cooling cycles	Scheduling and synchronization of chambers are optimized by artificial intelligence.
Product demand	Changing demand for products can be easily accommodated. Possible of making multiple solar panels with different structures.	Difficult to make changes as the process recipes are fixed for the entire line.	Changing demand for products can be easily accommodated. Possible of making multiple solar panels with different structures at the same time.
Equipment fouling	Tolerable to significant equipment fouling because cleaning / fixing of equipment is a standard operating procedure. Throughput can be affected when individual plasma-box fails in the process tower.	Significant fouling in continuous operations is a serious problem and difficult to handle. Sometimes significant fouling requires shutting down of the entire production line.	Fouling chamber can be by-passed or replaced with similar chambers, thus minimizing the adverse effect to the throughput.

Table 2. Comparison of three thin film solar module process flow types

Continuous deposition of the multilayer structure is realized in a roll-to-roll manner, which ensures stable chamber conditions for consistent film growth for large volume production. United Solar, Energy Conversion Devices (ECD), and Xunlight took this type of growth configuration. For example, the ECD 30 MW a-Si process line consists of nine series-connected chambers with gas gates that isolate dopant gases between chambers (Fig. 11b)

(Izu and Ellison 2003). The film deposition substrates are 2.6 km long, 36 cm wide, 127 μm thick stainless-steel rolls fed into the deposition system at constant speed. For quality assurance, online diagnostic systems are installed allowing for continuous monitoring of the layer thickness and characterization of the PV properties of the manufactured solar cells. A big advantage of the continuous process is that the substrate does not see the atmosphere during the process, and needs to be heated and cooled only at the beginning and last chamber, thus greatly saving the pumping time and energy cost. At the same time, all chambers continuously run at the optimized, stable states, thus depositing films with uniform and consistent properties. On the other hand, Since the deposition rate and thickness of each layer varies a lot (e.g., typical p-layers are < 20 nm while the μc-i layer is normally 1-2 μm), the deposition time in each chamber are very different. Limited by a constant substrate roll feeding speed, the chamber for growing i-layers are much longer than the doped layer chamber. In fact, this 30 MW system is 90 m long.

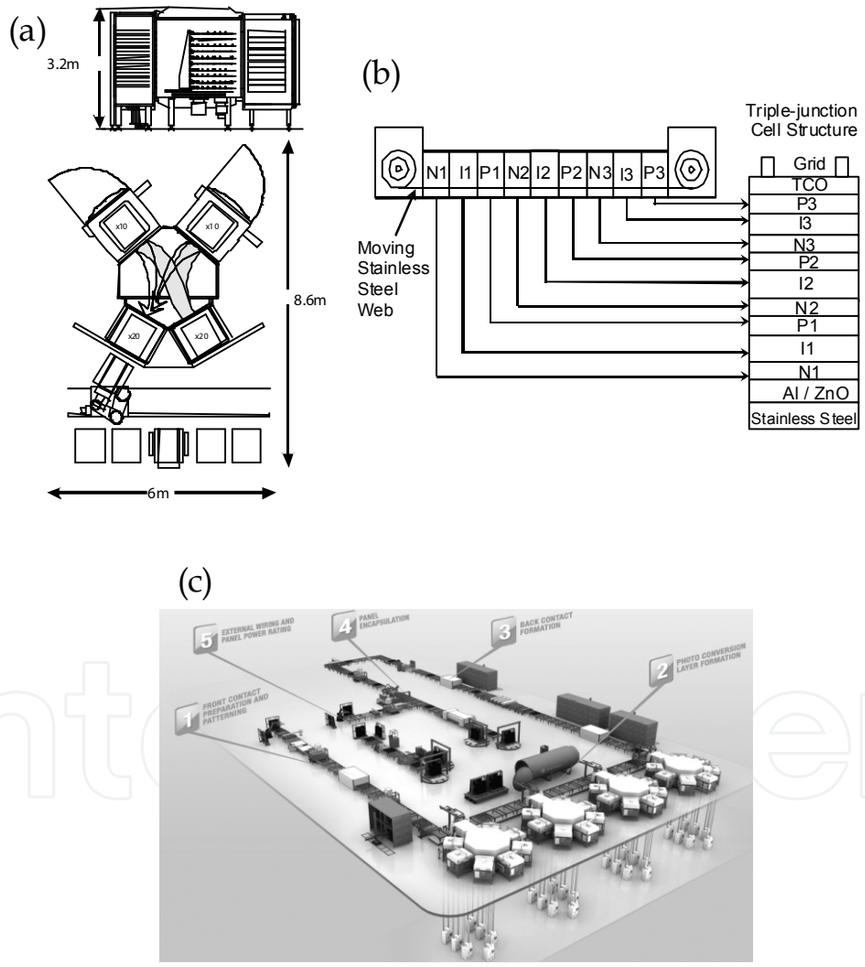

Fig. 11. Typical process systems used for Si thin film solar cell manufacturing. a) Batch process. Schematic side and top view of an Oerlikon KAI-20 1200 PECVD process system for a-Si deposition (Kroll et al. 2007). b) Linear Process. Schematic diagram of a United Solar Ovonic Corporation roll-to-roll a-Si:H alloy triple-junction solar cell processor (Yang et al. 2005). c) Hybrid (batch plus linear) process. Schematics of a Applied Materials SunFab thin film production line (Applied Materials 2010).

The hybrid-process system is designed to combine the advantages of batch and continuous processes. In this configuration, separated chambers are used like those in batch process, but individual substrates are fed into different chambers for optimal chamber utilization. Each substrate sees a queue of different process chambers like that in continuous process. Applied Materials configured its SunFab in the hybrid mode, where a group of several process chambers construct a functional cluster unit sharing a heating chamber and a center transfer robot (Fig. 11c). Each cluster is focused on a group of related functional layers (e.g., layers comprising a subcell in a multi-junction structure), and deposition of the multi-junction stack is realized by going through clusters. In this configuration, each chamber can have flexible deposition time, and the flow of substrates and synchronization of chambers are controlled by artificial intelligence algorithm for optimal system throughput (Applied Materials 2010; Bourzac 2010). This process flow combines the advantages of small footprint, easy maintenance and high production throughput, and provides flexible system configuration for versatile panel fabrication.

There are a number of considerations to weigh when deciding among batch, continuous or hybrid processes, and some of the major reasons are listed in Table 2. Generally, small production volumes favor the batch process type while continuous process is more suitable for high volume production. Capital investment cost of a batch or hybrid process system is also usually lower than the continuous process because the same equipment can be used for multiple unit operations and can be reconfigured easily for a wide variety of panel structures, though the operating labor costs and utility costs tend to be high for the former two systems (Turton et al. 2008). The continuous configuration is also more favored for 'substrate' type solar cells on metal foil substrates in a roll-to-roll deposition (Izu and Ellison 2003). Though the comparisons in Table 2 generally holds true, it is also possible that the configuration works for one solar plant may not be the best choice of another, as each plant differs at production scale, materials supply, geological confinement and many other practical characters.

5. Conclusion

In this chapter, the cost structures of a-Si/µc-Si solar modules has been described with analysis of the multilayer cell structure and module production. The monolithically integrated structure is described with explanations of layer functions. The industrial fabrication of large-area modules are introduced, including FEOL and BEOL process steps.

Module costs around half of the total thin film PV system. We analyzed the factors affecting the module efficiency and cost in terms of energy consumption, equipment investment, spending on direct material, labor and freight cost. To probe strategies of efficiency improvement, we started from the introduction of the Si p-i-n junction structure and the front/back contacts, and discussed the light absorption and its enhancement with light trapping. The photocurrent generation is achieved by effective capture of the incident solar photons, and conversion into free electrons and holes by the build-in field of the p-i-n junction. Resistance loss during photocurrent collections is minimized by the conductive front and back contact layers. At the meantime, enhancing the light absorption within thin layers is achieved using band gap engineering of the absorbing layer and optical trapping of the front/back contact layers.

Fabrication of large-area tin film solar panels are the key to increasing the production volume and reducing the $/Wp of modules. State-of-the-art fabrication includes FEOL and

BEOL process steps. In the FEOL processes, glass substrates are subsequently coated with functional layers, i.e., the a-Si/μc-Si layers by PECVD, TCO and reflector layers are grown by PVD or CVD. The monolithically integrated module structure is achieved by laser scribing of individual layers. In the BEOL processes, the panels are cut and encapsulated. Electrical wiring are also finished in the BEOL steps. The batch, linear, and hybrid process flow schemes are compared with actual factory examples.

Thin film a-Si/μc-Si solar panels have been holding the largest market share among all produced thin film panels. The power conversion efficiency of these panels is likely to increase to above 12% in the near future, but not exceed that achieved in crystalline cells. Advantages such as large-area, low-cost fabrication, and demonstrated field performance, nevertheless, render a-Si/μc-Si thin film technology attractive for large-area deployment like in solar power plants. In particular with the uncertain elemental supply becomes an issue for CdTe and CIS cells that might impair the sustainability of those PV products (Fthenakis 2009), thin film a-Si/μc-Si is likely to have long-term potential for providing energy supply in an even larger scale. Improvements on efficiency and stability would continue to drive the research in this area, while panel manufacturing will continue to be optimized for achieving lower production cost and optimal $/Wp.

6. References

Agashe, C., et al. (2004). Efforts to improve carrier mobility in radio frequency sputtered aluminum doped zinc oxide films. *Journal of Applied Physics* Vol. 95, No. 4: pp. 1911-1917, ISSN 2158-3226

Applied Materials, Inc. (2010). Applied Materials Solar, Last accessed 2011, Available from http://www.appliedmaterials.com/technologies/solar

Beck, N., et al. (1996). Mobility lifetime product---A tool for correlating a-Si:H film properties and solar cell performances. *Journal of Applied Physics* Vol. 79, No. 12: pp. 9361-9368, ISSN 2158-3226

Berger, O., et al. (2007). Commercial white paint as back surface reflector for thin-film solar cells. *Solar Energy Materials and Solar Cells* Vol. 91, No. 13: pp. 1215-1221, ISSN 0927-0248

Beyer, W., et al. (2007). Transparent conducting oxide films for thin film silicon photovoltaics. *Thin Solid Films* Vol. 516, No. 2-4: pp. 147-154, ISSN 0040-6090

Bhan, M. K., et al. (2010). Scaling single-junction a-Si thin-film PV technology to the next level. *Photovoltaics International* Vol. 7: pp. 101-106, ISSN 1757-1197

Borrajo, J. P., et al. (2009). Laser scribing of very large 2,6m x 2,2m a-Si: H thin film photovoltaic modules. *Processings of Spanish Conference on Electron Devices, 2009*, pp. 402-405, 11-13 Feb. 2009

Bourzac, K. (2010). Scaling Up Solar Power. *Technology Review* Vol. 113, No. 2: pp. 84-86, ISSN 1099274X

Bruno, G., et al. (1995). *Plasma Deposition of Amorphous Silicon-Based Materials (Plasma-Materials Interactions)*. Academic Press ISBN 978-0121379407

Droz, C., et al. (2000). Electronic transport in hydrogenated microcrystalline silicon: similarities with amorphous silicon. *Journal of Non-Crystalline Solids* Vol. 266-269, No. Part 1: pp. 319-324, ISSN 0022-3093

Fortunato, E., et al. (2007). Transparent Conducting Oxides for Photovoltaics. *MRS BULLETIN* Vol. 32, No. 3: pp. 242-247, ISSN 0883-7694

Fthenakis, V. (2009). Sustainability of photovoltaics: The case for thin-film solar cells. *Renewable and Sustainable Energy Reviews* Vol. 13, No. 9: pp. 2746-2750, ISSN 1364-0321

Green, M. A. (2007). *Third Generation Photovoltaics: Advanced Solar Energy Conversion* Springer, ISBN 978-3540265627, New York

Hegedus, S. S. & Luque, A., Eds. (2003). *Status, Trends, Challenges and the Bright Future of Solar Electricity from Photovoltaics*. John Wiley & Sons Inc., ISBN 0-471-49196-9, Chippenham, Great Britain

Izu, M. & Ellison, T. (2003). Roll-to-roll manufacturing of amorphous silicon alloy solar cells with in situ cell performance diagnostics. *Solar Energy Materials and Solar Cells* Vol. 78, No. 1-4: pp. 613-626, ISSN 0927-0248

Jäger-Waldau, A. (2007). Status and Perspectives of Thin Film Solar Cell Production. *Processings of 3rd International Photovoltaic Industry Workshop on Thin Films*, EC JRC Ispra, November 22-23, 2007

Johnson, T. R., et al. (2003). Investigation of the Causes and Variation of Leakage Currents in Amorphous Silicon P-I-N Diodes. *Materials Research Society Symposium - Proceedings* Vol. 762: pp. A7.7.1-A7.7.6, ISSN 0272-9172

Jorgensen, G. J., et al. (2006). Moisture transport, adhesion, and corrosion protection of PV module packaging materials. *Solar Energy Materials and Solar Cells* Vol. 90, No. 16: pp. 2739-2775, ISSN 0927-0248

Kambe, M., et al. (2009). Improved light-trapping effect in a-Si:H / µc-Si:H tandem solar cells by using high haze SnO_2:F thin films. *Processings of Photovoltaic Specialists Conference (PVSC), 2009 34th IEEE*, pp. 001663-001666, Philadelphia, USA, June 2009

Kessels, W. M. M., et al. (2001). Hydrogenated amorphous silicon deposited at very high growth rates by an expanding Ar-H2-SiH4 plasma. *Journal of Applied Physics* Vol. 89, No. 4: pp. 2404-2413, ISSN 2158-3226

Klein, S., et al. (2002). High Efficiency Thin Film Solar Cells with Intrinsic Microcrystalline Silicon Prepared by Hot Wire CVD. *Materials Research Society Symposia Proceedings* Vol. 715: pp. A26.22, ISSN 0272-9172

Kolodziej, A. (2004). Staebler-Wronski effect in amorphous silicon and its alloys. *Opto-Electronics Review* Vol. 12, No. 1: pp. 21-32, ISSN 1230-3402

Kroll, U., et al. (2007). Status of thin film silicon PV developments at Oerlikon solar. *Processings of 22nd European Photovoltaic Solar Energy Conference*, pp. 1795-1800, Milan, Italy

Luft, W. & Tsuo, Y. S. (1993). *Hydrogenated amorphous silicon alloy deposition processes*. CRC Press, ISBN 978-0824791469, New York

Mai, Y., et al. (2005). Microcrystalline silicon solar cells deposited at high rates. *Journal of Applied Physics* Vol. 97, No. 11: pp. 114913-114912, ISSN 2158-3226

Mehta, S. (2010). Thin film 2010: market outlook to 2015

Meier, J., et al. (2010). From R&D to Large-Area Modules at Oerlikon Solar. *Materials Research Society Symposia Proceedings* Vol. 1245: pp. 1245-A01-02, ISSN 0272-9172

Meier, J., et al. (2007). UP-scaling process of thin film silicon solar cells and modules in industrial pecvd kai systems. *Conference Record of the 2006 IEEE 4th World Conference on Photovoltaic Energy Conversion, WCPEC-4*, pp. 1720-1723

Meier, J., et al. (2005). Progress in up-scaling of thin film silicon solar cells by large-area PECVD KAI systems. *Conference Record of the Thirty-first IEEE Photovoltaic Specialists Conference, 2005*, pp. 1464-1467

Müller, J., et al. (2004). TCO and light trapping in silicon thin film solar cells. *Solar Energy* Vol. 77, No. 6: pp. 917-930, ISSN 0038-092X

Nishimiya, T., et al. (2008). Large area VHF plasma production by a balanced power feeding method. *Thin Solid Films* Vol. 516, No. 13: pp. 4430-4434, ISSN 0040-6090

Rath, J. K., et al. (2010). Transparent conducting oxide layers for thin film silicon solar cells. *Thin Solid Films* Vol. 518, No. 24 SUPPL.: pp. e129-e135, ISSN 0040-6090

Repmann, T., et al. (2007). Production equipment for large area deposition of amorphous and microcrystalline silicon thin-film solar cells. *Conference Record of the 2006 IEEE 4th World Conference on Photovoltaic Energy Conversion, WCPEC-4*, pp. 1724-1727

Sato, K., et al. (1992). Highly textured SnO_2:F TCO films for a-Si solar cells. *Reports of the Research Laboratory, Asahi Glass Co., Ltd.* Vol. 42, No.: pp. 129-137, ISSN 0004-4210

Schroeder, B. (2003). Status report: Solar cell related research and development using amorphous and microcrystalline silicon deposited by HW(Cat)CVD. *Thin Solid Films* Vol. 430, No. 1-2: pp. 1-6, ISSN 0040-6090

Schropp, R. E. I. (2006). *Amorphous (Protocrystalline) and Microcrystalline Thin Film Silicon Solar Cells*. Elsevier B. V., ISBN 9780444528445

Schropp, R. E. I. & Zeman, M. (1998). *Amorphous and Microcrystalline Silicon Solar Cells*. Kluwer Academic Publishers, ISBN 978-0792383178 Boston

Shah, A. V., et al. (2004). Thin-film silicon solar cell technology. *Progress in Photovoltaics: Research and Applications* Vol. 12, No. 2-3: pp. 113-142, ISSN 1099-159X

Shinohara, W., et al. (2006). Applications of laser patterning to fabricate innovative thin-film silicon solar cells. *Processings of SPIE*, Vol. 6107, pp. 61070J-1-18

Sun, H., et al. (2009). End-To-End Turn-Key Large Scale Mass Production Solution for Generation 1 & 2 Thin Film Silicon Solar Module. *Proceedings of ISES World Congress 2007 (Vol. I – Vol. V)*, pp. 1220-1223

Turton, R., et al. (2008). *Analysis, Synthesis, and Design of Chemical Processes*. Prentice Hall, ISBN 0-13-512966-4, Westford, MA

Yamamoto, K., et al. (2006). High Efficiency Thin Film Silicon Hybrid Cell and Module with Newly Developed Innovative Interlayer. *Conference Record of the 2006 IEEE 4th World Conference on Photovoltaic Energy Conversion*, pp. 1489-1492

Yang, F., et al. (2009). Uniform growth of a-Si:H / μc-Si:H tandem junction solar cells over 5.7m² substrates. *Processings of 34th IEEE Photovoltaic Specialists Conference*, pp. 1541-1545, Philadelphia, PA

Yang, J., et al. (2005). Amorphous and nanocrystalline silicon-based multi-junction solar cells. *Thin Solid Films* Vol. 487, No. 1-2: pp. 162-169, ISSN 0040-6090

Yang, Y.-T., et al. (2007). The Latest Plasma-Enhanced Chemical-Vapor Deposition Technology for Large-Size Processing. *Journal of Display Technology* Vol. 3, No. 4: pp. 386-391, ISSN 1551-319X

Young, R. (2010). PV Cell Capacity, Shipment and Company Profile Report, IMS Research

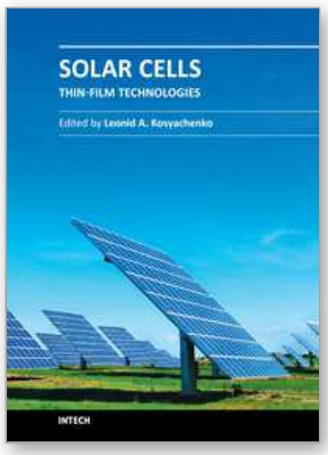

Solar Cells - Thin-Film Technologies

Edited by Prof. Leonid A. Kosyachenko

ISBN 978-953-307-570-9
Hard cover, 456 pages
Publisher InTech
Published online 02, November, 2011
Published in print edition November, 2011

The first book of this four-volume edition is dedicated to one of the most promising areas of photovoltaics, which has already reached a large-scale production of the second-generation thin-film solar modules and has resulted in building the powerful solar plants in several countries around the world. Thin-film technologies using direct-gap semiconductors such as CIGS and CdTe offer the lowest manufacturing costs and are becoming more prevalent in the industry allowing to improve manufacturability of the production at significantly larger scales than for wafer or ribbon Si modules. It is only a matter of time before thin films like CIGS and CdTe will replace wafer-based silicon solar cells as the dominant photovoltaic technology. Photoelectric efficiency of thin-film solar modules is still far from the theoretical limit. The scientific and technological problems of increasing this key parameter of the solar cell are discussed in several chapters of this volume.

InTech Europe
University Campus STeP Ri
Slavka Krautzeka 83/A
51000 Rijeka, Croatia
Phone: +385 (51) 770 447
Fax: +385 (51) 686 166
www.intechopen.com

InTech China
Unit 405, Office Block, Hotel Equatorial Shanghai
No.65, Yan An Road (West), Shanghai, 200040, China
中国上海市延安西路65号上海国际贵都大饭店办公楼405单元
Phone: +86-21-62489820
Fax: +86-21-62489821

IntechOpen